

Chapter 1

Independent evaluation of the ability of spaceborne radar and lidar to retrieve the microphysical and radiative properties of ice clouds

Summary. The combination of radar and lidar in space offers the unique potential to retrieve vertical profiles of ice water content and particle size globally, and two algorithms developed recently claim to have overcome the principal difficulty with this approach, that of correcting the lidar signal for extinction. In this chapter “blind tests” of these two algorithms are carried out, using simulated but realistic 94-GHz radar and 355-nm lidar backscatter profiles derived from aircraft-measured size spectra, and including the effects of molecular scattering, multiple scattering and instrument noise. Then radiation calculations are performed on the true and retrieved microphysical profiles to estimate the accuracy with which the radiative flux profiles could be inferred from such retrievals. It is found that the visible extinction profile can be retrieved with remarkable accuracy through most of the depth of the cloud, independently of assumptions on the nature of the size distribution, the habit of the particles, the absolute value of the extinction-to-backscatter ratio or even errors in instrument calibration. However, errors in retrieved optical depth can exceed 1, which changes the short-wave fluxes by several tens of W m^{-2} , although this is mostly due to errors at the far end of the profile and the optical depth down to 400 m above the height of the lowest lidar return is typically retrieved to better than 0.2. Long-wave fluxes are much less sensitive to errors in total optical depth, and may generally be calculated to an accuracy of better than 2 W m^{-2} throughout the profile. Note that it is essential for retrieval algorithms to account for the effects of lidar multiple scattering, as if this is neglected then the optical depth is underestimated by around 80%, with consequent gross underestimation of cloud radiative effects. Unlike extinction coefficient, the inferred ice water content and particle size do depend significantly on the assumed mass-size relationship (a problem common to all remote retrieval algorithms), but it is found that the radiative fluxes are almost completely determined by the extinction profile, and if this is correct then errors in these other parameters have only a small effect in the short-wave (around 6% compared to clear-sky) and a negligible effect in the long-wave.

1.1 Introduction

Ice clouds play an important role in the radiation budget of the earth (Liou 1986, Stephens et al. 1990), so it is of major concern that the vertically integrated ice content simulated by the various climate models currently in use spans an order of magnitude (Stephens et al. 2002). Active remote sensing from space offers the best hope of reducing this uncertainty, with the added advantage that the measurements would be at a high vertical resolution. Brown et al. (1995) estimated that spaceborne 94-GHz radar should

be able to retrieve ice water content (IWC) to within a factor of two (with the error due to the fact that the radar measures a high moment of the size distribution), but that if information were available on particle size then this could be reduced to around $\pm 40\%$. Liu and Illingworth (2000) showed that simple incorporation of temperature would make retrieved IWC more accurate, exploiting the fact that ice particles in warmer clouds tend to be larger. Hogan and Illingworth (1999) suggested supplementing the 94-GHz radar with one at around 215-GHz, such that particles larger than around $200 \mu\text{m}$ would scatter outside the Rayleigh regime at the higher frequency and the ratio of reflectivities would provide information on particle size.

A more attractive solution is to combine radar and lidar; the much greater difference in the size dependence of the backscatter yields more accurate size measurements and the ability to size much smaller particles. Furthermore, the use of a wavelength that lies within the gamut of important natural radiation implies that the radiative parameters of the clouds may be more accurately inferred. With the scheduled launch of the CloudSat radar and the Calipso lidar in 2005 (Stephens et al. 2002), and the proposed EarthCARE mission (Earth Cloud, Aerosol and Radiation Explorer) involving a cloud radar and lidar on the same platform later in the decade (ESA 2001), the prospects for such measurements from space in the near future are excellent.

Intrieri et al. (1993), Mace et al. (1999) and Wang and Sassen (2002) have used the combined radar-lidar approach to derive the properties of ice clouds from ground based instruments, but a problem that soon becomes apparent in more optically thick clouds is extinction of the lidar signal; if uncorrected, the inferred particle size quickly becomes too large and the ice water content too small as the lidar echo is diminished. Attempting to correct the lidar for extinction by simply assuming a relationship between backscatter and extinction is problematic as small changes in the relationship yield rapidly diverging extinction profiles, and from the lidar alone there is insufficient information to choose between them, with the exception of the special case that the lidar is able to detect the molecular return at the far side of the cloud. A simple but powerful solution is to make use of the radar information in the extinction-correction stage, as only a very small range of these possible extinction profiles yields plausible profiles of particle size or number concentration when combined with the radar. This idea has led to the development of two different algorithms, one by Donovan and van Lammeren (2001) at the Royal Dutch Meteorological Institute (KNMI), and the other by Tinel et al. (2000) at the *Institut Pierre Simon Laplace* (IPSL) in France.

The purpose of this chapter is to assess the skill of these two algorithms in retrieving profiles of IWC, visible extinction coefficient (α) and effective radius (r_e), given the instrument characteristics of the proposed EarthCARE satellite. The parameters of interest are not independent, being linked by (Foot 1988)

$$r_e = \frac{3 \text{ IWC}}{2 \rho_i \alpha}, \quad (1.1)$$

where ρ_i is the density of solid ice. Visible extinction coefficient is the most important parameter for determining the radiative properties of the cloud both in the short-wave and the thermal infrared (since the infrared extinction is approximately equal to $\alpha/2$). It is also the parameter that can be most accurately determined from the combination of lidar and radar. Numerical models, however, usually hold IWC as a prognostic variable (or alternatively total condensed water from which ice fraction is diagnosed), and must parameterize effective radius in order to obtain extinction in the radiation scheme. Asymmetry factor and single-scattering albedo are parameterized as a function of effective radius.

Independent evaluation of the algorithms was achieved by means of “blind tests”; Robin Hogan used ice particle size distributions measured during aircraft descents through mid-latitude frontal ice cloud to generate the radar and lidar backscatter profiles that would be measured from space. These

were then provided to David Donovan (KNMI) and Claire Tinel (IPSL) who applied their codes with no knowledge of the original measurements and only limited knowledge of the assumptions that had been made in the synthesis of the radar and lidar data. The retrieved profiles of IWC, α and r_e were then compared to the “true” values. Finally, one-dimensional radiation calculations were performed to determine the impact of any errors in the retrievals on the long-wave and short-wave radiative flux profiles.

Two blind tests were performed. In the first, the instruments were assumed to be noise-free and almost infinitely sensitive, and the lidar extinction-to-backscatter ratio, k , was allowed to vary by as much as a factor of two within each profile (with the algorithms knowing nothing about the nature of the k). This way the ability of the algorithms to recover extinction in clouds with a one-way optical depth as much as 7 was evaluated. Their success prompted a more realistic second blind test, in which instrumental noise was added to a new set of profiles, along with the effects of lidar multiple and molecular scattering.

In section 1.2 the principles behind the KNMI and IPSL algorithms are outlined. Rather than providing an exhaustive mathematical treatment (which may be found elsewhere), we concentrate on explaining the physical basis behind them, what they have in common and in what ways they differ. The generation of the profiles from aircraft data is described in section 1.3. Then in section 1.4, the results of the two blind tests are analyzed in terms of the sensitivity of the retrievals to each of the factors that introduce error. The impacts of these errors for the implied radiative properties of the clouds are then reported in section 1.5.

1.2 Description of the algorithms

1.2.1 Theoretical background

In its simplest terms, the principle behind the use of radar and lidar to retrieve the microphysical properties of clouds is straightforward: radar measures radar reflectivity factor, Z , which is approximately proportional to particle size to the power of six, while the lidar return is related to particle size to the power of two. Therefore the ratio of the two is proportional to the fourth power of size, enabling size to be retrieved very accurately. With a suitable assumption regarding the nature of the size distribution (such as it being a gamma distribution with a particular shape parameter), all other moments of the distribution (such as water content) and measures of size (such as effective radius) may be estimated.

O’Connor et al. (2003) recently took this approach to retrieve the parameters of drizzle falling beneath stratocumulus cloud. The radar and lidar scattering properties of liquid droplets can be calculated with a high degree of accuracy, enabling the measurements to be interpreted unambiguously, but in the case of ice clouds the particles occur in a multitude of different habits which are generally unknown to a remote sensing algorithm, and the radar and lidar backscattering properties cannot be calculated exactly.

The radar reflectivity factor of ice clouds is usually expressed assuming the particles to be spheres of diameter D consisting of a homogeneous mixture of ice and air with a density that varies with D alone (e.g. Hogan and Illingworth 1999):

$$Z = \frac{1}{0.93} \int_0^\infty n(D) |K(D)|^2 D^6 \gamma(D) dD, \quad (1.2)$$

where $n(D)$ is the number concentration of particles with diameter between D and $D + dD$, $|K|^2$ is the dielectric factor (proportional to density squared) and γ is the Mie-to-Rayleigh backscatter ratio. In reality ice particles are not spheres and a simple density relationship will not be strictly applicable to all

the particles in a radar sample volume, so we generalize this formula to a summation over a unit volume of arbitrary ice particles:

$$Z = \frac{|K_i|^2}{0.93} \left(\frac{6}{\pi \rho_i} \right)^2 \sum_j m_j^2 \gamma_j, \quad (1.3)$$

where m_j is the mass of particle j and $|K_i|^2$ is the dielectric factor of solid ice (with the value 0.174). The γ_j factor is now the ratio of the actual backscattering cross-section to that predicted by Rayleigh theory, and in principle need not be calculated using Mie theory. In the Rayleigh-scattering limit it is much more convenient to consider reflectivity as simply proportional to mass squared as in (1.3), than to use (1.2) and have to work with the concepts of “diameter” and “density”, which are ill-defined for arbitrarily shaped particles. Note that radar attenuation by ice clouds can generally be considered negligible up to 94 GHz (Hogan and Illingworth 1999).

The parameter we wish to obtain from lidar is visible extinction coefficient, which in the geometric optics approximation is simply twice the sum of particle cross-sectional areas (A) in a unit volume:

$$\alpha = 2 \sum_j A_j. \quad (1.4)$$

The main problem to overcome in the retrieval is that the lidar return itself suffers extinction by the cloud, and this effect must be corrected before the measurements can be used in combination with radar to estimate particle size. Lidar essentially measures attenuated lidar backscatter coefficient (β'), which for a near-nadir viewing instrument, neglecting the molecular contributions to the extinction and backscatter and assuming single scattering, is given by

$$\beta'(z) = \beta(z) \exp \left[-2 \int_z^{z_0} \alpha(z') dz' \right], \quad (1.5)$$

where $\beta(z)$ is the unattenuated backscatter coefficient at height z , and z_0 is the height of the instrument. We want to retrieve the extinction profile. If the extinction to backscatter ratio, $k = \alpha/\beta$ is assumed constant through the profile, then it can be shown that

$$\alpha(z) = \beta'(z) \left[\frac{1}{k} - 2 \int_z^{z_0} \beta'(z') dz' \right]^{-1}. \quad (1.6)$$

The problem is that for all but the most optically thin clouds, the retrieved α profile is extremely sensitive to the exact value of k assumed. This is particularly true at the far end of the cloud. Klett (1985) showed that if the value of α at the far end of the profile could be estimated, or if the total optical depth of the cloud was known, then this problem could be overcome and a stable profile of α retrieved. If the molecular scattering at the far side of the cloud is detectable then it can be used to estimate cloud optical depth and this approach becomes very powerful, but for optical depths greater than around 2 the molecular signal at 355 nm is completely extinguished. At longer wavelengths the molecular signal is much weaker and total extinction occurs for even lower optical depths. The difficulty is then that from lidar alone there is no way of knowing the extinction coefficient at the far end of the cloud, and extinction coefficients in ice clouds vary over many orders of magnitude.

The solution adopted by both the KNMI and IPSL algorithms is to use the information available from the radar in the correction procedure: essentially, only a very narrow range of k in (1.6) will produce an α profile that, when combined with the radar, produces a plausible profile of meteorological variables. This approach is a departure from that of Wang and Sassen (2002) and others, who attempt to somehow correct the lidar for extinction independently, before combining with radar.

1.2.2 KNMI lidar extinction correction

The KNMI algorithm hypothesizes that the most likely α profile is that which results in the least fluctuation of retrieved particle size at the far end of the cloud. It is described in detail by Donovan and van Lammeren (2001). Rather than using r_e as defined in (1.1), which involves assumptions on ice particle habits, a “radar-lidar effective radius”, r'_e , is used:

$$r'_e = \left(\frac{0.93 \pi Z}{|K_i|^2 8 \alpha} \right)^{\frac{1}{4}}. \quad (1.7)$$

The coefficients ensure that in the simple case of solid, Rayleigh-scattering ice spheres of radius r , this expression reduces to

$$r'_e = [\langle r^6 \rangle / \langle r^2 \rangle]^{\frac{1}{4}}. \quad (1.8)$$

The parallel with the “classical” definition of effective radius in the case of liquid water clouds of $r_e = \langle r^3 \rangle / \langle r^2 \rangle$ is obvious.

A cost function is defined which penalizes gradients in $\ln(r'_e)$ in the furthest few gates of the profile. An iterative procedure is then used to find the k value in (1.6) that minimizes this cost function, although note that the algorithm may also be formulated in terms of either the total optical depth or the α value at the far end of the profile. It should be pointed out that because the natural logarithm of r'_e is taken, the power of $\frac{1}{4}$ in (1.7) has no effect on the retrieval; effectively we are finding the α profile that simply minimizes variations in the ratio of Z to α at the far end of the cloud.

1.2.3 IPSL lidar extinction correction

The IPSL algorithm is similar to the KNMI algorithm except that it hypothesizes that the correct α retrieval is that which results in the least fluctuation of particle number concentration; the full details are described by Tinel et al. (2000). Rather than attempting to derive the actual number concentration, the concept of a normalized number concentration parameter (Testud et al. 2001, Illingworth and Blackman 2002), N_0^* , is adopted. In the case of ice clouds it may be defined as

$$N_0^* = \left(\frac{4}{D_m} \right)^4 \frac{\text{IWC}}{\pi \rho_w}, \quad (1.9)$$

where D_m is the volume-weighted mean diameter and ρ_w is the density of liquid water. Analysis of aircraft data shows that when various moments of the distribution are normalized by N_0^* , very precise power-law relationships exist between them. For example, Tinel (2002) derived the following relationship between α (in m^{-1}) and Z (in $\text{mm}^6 \text{m}^{-3}$):

$$\frac{\alpha}{N_0^*} = 1.22 \times 10^{-5} \left(\frac{Z}{N_0^*} \right)^{0.415}, \quad (1.10)$$

where N_0^* has the units m^{-4} . This can be rearranged to

$$N_0^* = 2.50 \times 10^8 \frac{\alpha^{1.71}}{Z^{0.71}}. \quad (1.11)$$

An iterative procedure then finds the α profile that yields the least variation of N_0^* with range.

So despite appearing to be based on very different principles, the KNMI and IPSL algorithms effectively retrieve the extinction profile in a very similar way: by finding the solution that minimizes variations in the ratio of some power of Z to some power of α . Whether the exact values of these powers are significant will be determined in section 1.4.2.

1.2.4 Correction for lidar multiple scattering

A further problem to address is that the light from spaceborne lidars can undergo more than one scattering event before being returned to the detector, which manifests itself as a range-dependent enhancement of the measured backscatter. The KNMI algorithm has the capability to account for this effect using the multiple-scattering model of Eloranta (1998), coupled with knowledge of the properties of the lidar in question. Essentially the use of an analytical formula such as (1.4) to determine the α profile for a given measured backscatter profile and boundary value is replaced by an iterative numerical solution that incorporates the effect of multiple scattering (Donovan and van Lammeren 2001). The IPSL algorithm currently has no capability to correct for multiple scattering. The significance of this omission is found in Blind Test 2 in which the effects of multiple scattering are included in the simulated profiles.

1.2.5 Estimation of IWC and effective radius

The last step in the retrieval is to use the combination of Z and α to estimate IWC and r_e . From (1.1) it can be seen that an estimate of one of IWC or r_e implies an estimate of the other. The KNMI algorithm uses the results of Donovan and van Lammeren (2001), who derived relationships between r_e and r'_e by simulating them for idealized monomodal and bimodal distributions of particles with various assumed mass-size relationships taken from the literature. Where not otherwise stated, a single gamma distribution is assumed with the Francis et al. (1998) mass-area relationship. Donovan and van Lammeren (2001) noted a span of a factor of two in retrieved r_e between the various combinations of size distribution and mass-size relationship.

The IPSL algorithm, on the other hand, makes use of the N_0^* concept. Tinel (2002) used aircraft data to find an empirical relationship between IWC/N_0^* and Z/N_0^* , which is used to infer the profile of IWC from observed Z and retrieved N_0^* . There was very little scatter in the aircraft data presented by Tinel (2002), implying a very accurate retrieval of IWC, but Z and IWC are calculated assuming a fixed mass-size relationship and deviations from this expression in real clouds will feed through to errors in IWC and r_e , in the same way as for the KNMI algorithm. These sensitivities are explored further in sections 1.4.4 and 1.4.7.

1.3 Generation of synthetic radar and lidar profiles

1.3.1 Blind Test 1: profiles 1–5

The radar and lidar profiles in the first blind test were simulated from in situ data taken by the UK Met Office C-130 aircraft during five Lagrangian descents in frontal clouds around the British Isles. The flight patterns consisted of short straight and level runs separated by descents of around 500 m, with the total physical cloud thicknesses ranging between 3 and 6 km. Ice particle size distributions were measured by the Particle Measuring System 2D cloud and precipitation probes, spanning the diameter range 25–6400 μm , and were available binned by both cross-sectional area, A , and the mean of the maximum dimensions measured parallel and perpendicular to the photodiode arrays, D . The distributions were far from monomodal, and in fact the same data were used by Field (2000) to demonstrate the evolution of bimodal size distributions due to the effects of aggregation. From each straight and level run a single 5-s-averaged size distribution was extracted, corresponding to around 500 m in the horizontal. This is comparable with the horizontal resolution at which spaceborne radar-lidar retrievals would be performed.

The size distributions binned by area were used to calculate the various parameters of interest. Visible extinction was calculated using (1.4). In calculating ice water content, the relationship of Francis

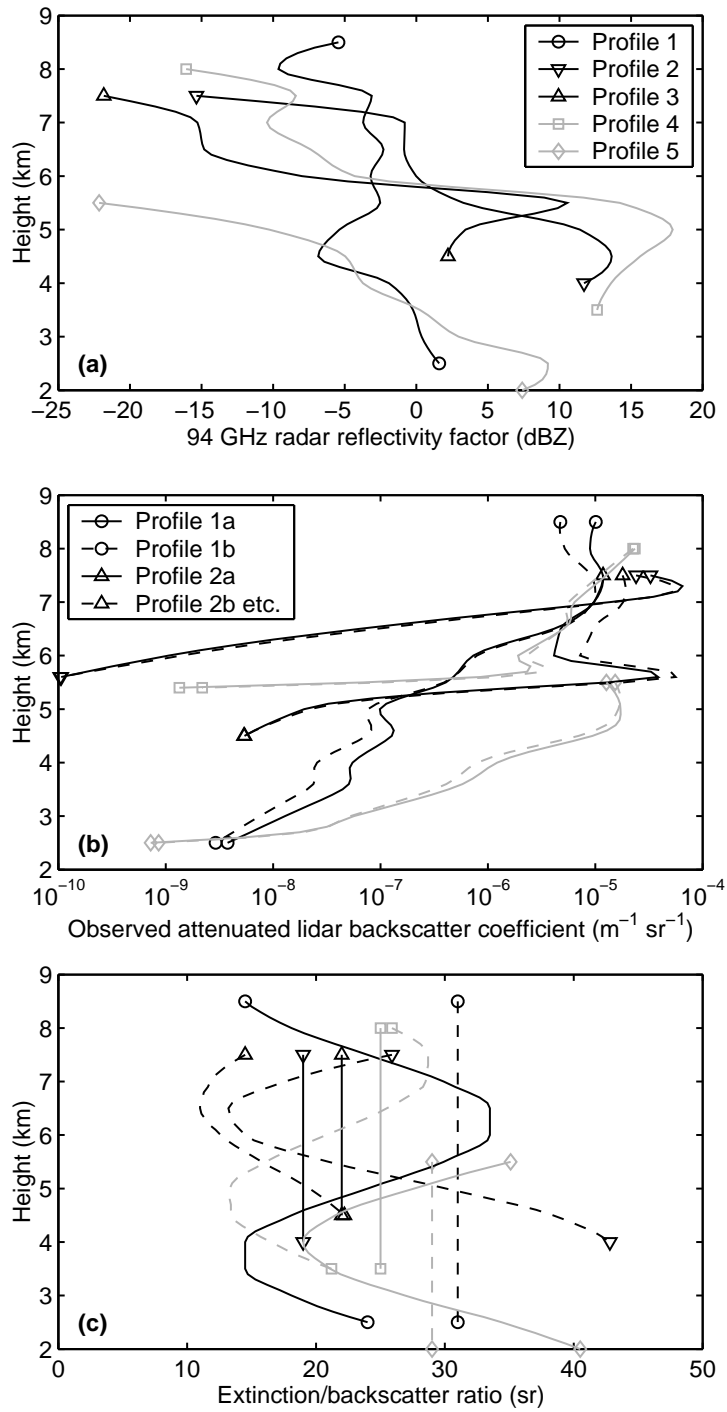


Figure 1.1: Profiles used in Blind Test 1: (a) radar reflectivity factor Z , (b) attenuated lidar backscatter coefficient β' and (c) extinction/backscatter ratio k . The k profiles were not available to the algorithms.

et al. (1998) was used to determine the ice particle mass from its cross-sectional area. Effective radius was then calculated using (1.1). Radar reflectivity factor at 94 GHz was calculated by approximating the ice particles as spheres composed of a uniform mixture of ice and air with a diameter equal to the equivalent-area diameter $D_A = 2(A/\pi)^{1/2}$. Equation 1.3 was then applied using the same mass as in the IWC calculation, and using Mie theory to calculate γ from D_A .

In this way five profiles at a vertical resolution of 500 m were generated. The profiles of Z and α

were interpolated to 100 m using cubic splines in logarithmic space, thereby simulating the resolution that will be possible from space (albeit oversampled in the case of the radar). Finally, the attenuated backscatter that would be measured by the lidar (in the absence of molecular or multiple scattering) was calculated using (1.5). For each of the five profiles, two profiles of extinction-to-backscatter ratio k were employed, one constant with height and the other varying over around a factor of two, similar to the range found by Ansmann et al. (1992). The measured backscatter coefficients were truncated at a value of $10^{-10} \text{ m}^{-1} \text{ sr}^{-1}$, which affected profiles 2, 4 and 5. Note that this is much lower than can be measured by any real lidar, but it provides an ultimate test of the extinction-correction capabilities of the two algorithms.

Figure 1.1 shows the five reflectivity and ten backscatter profiles that were applied in the algorithms. Note that the algorithms had absolutely no knowledge of the k values (also shown in Fig. 1.1) that had been used.

1.3.2 Blind Test 2: profiles 6–10

As will be seen in sections 1.4.1 and 1.4.4, the first blind test demonstrated the impressive skill of both algorithms, but it omitted a number of instrumental and optical factors that will make radar-lidar retrievals from space more difficult. In Blind Test 2, these effects were simulated to provide a much more realistic and challenging test for the algorithms. Again, C-130 aircraft size spectra were used, this time from the European Cloud Radiation Experiment (EUCREX). The five new profiles (6–10) were intended to represent a 10-km dwell (1.4 s) from the EarthCARE satellite at an altitude of 400 km, with a 100-m vertical resolution.

As before the data were available by D and A . Profiles 7–9 used the mass-area relationship of Francis et al. (1998) as before, but profiles 6 and 10 used the data binned by D , coupled to the mass- D relationship of Brown and Francis (1995), for the calculations of both IWC and Z .

The 2D cloud probe is known to be somewhat unreliable for measuring particles smaller than $100 \mu\text{m}$ (Heymsfield and Baumgardner 1985), with the result that the ice water content in these small particles is underestimated by around a factor of 2.5 (McFarquhar and Heymsfield 1997). We correct for this effect using the same procedure as described by Hogan and Illingworth (2003), fitting a gamma distribution to the small particle mode. This removes the small-particle IWC bias but effectively makes the distribution more bimodal, so might be expected to increase the error of the retrievals.

Gaussian smoothing of the radar reflectivity profile calculated from the aircraft spectra is used to simulate 100-m oversampling of an impulse response function with a two-way half-power full width of 385 m. Random measurement errors are then added following Hogan and Illingworth (1999), assuming that 8400 independent samples are taken in 1.4 s and a thermal/instrument background noise of -22.1 dBZ . This yields a minimum-detectable signal of -38 dBZ at all altitudes. Generally the radar errors are small, particularly at large signal-to-noise ratio where they are only around $\pm 0.05 \text{ dB}$. Gaseous attenuation is not simulated as it is assumed to be characterized well enough that it could easily be corrected in real observations. The resulting profiles are shown in Fig. 1.2a.

The changes to the lidar profile in Blind Test 2 are much more drastic, as is evident in Fig. 1.2b. Firstly, the Rayleigh backscatter from the air molecules, β_{mol} , is added to the unattenuated backscatter coefficient profile assuming the following height dependence at 355 nm:

$$\beta_{\text{mol}}(z) = 8.1 \times 10^{-6} \exp(z/8000) \quad (1.12)$$

where β_{mol} has the units $\text{m}^{-1} \text{ sr}^{-1}$ and z is in m. It is assumed that the density profile of the atmosphere is known well enough that this would be possible to calculate accurately in a real retrieval, so it was

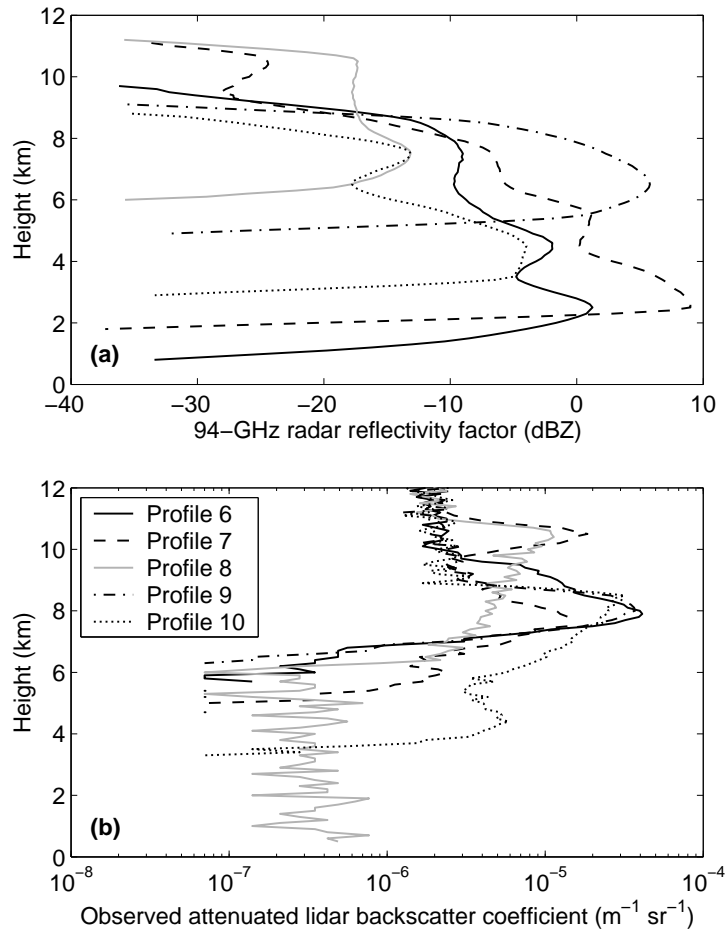


Figure 1.2: Profiles used in Blind Test 2: (a) radar reflectivity factor Z and (b) attenuated lidar backscatter coefficient β' .

available to the operators of the algorithms. For the same reason, the extinction of the lidar beam due to molecular scattering was not simulated. The molecular return is clearly visible at the top of the profiles shown in Fig. 1.2b, and in profile 8 at the bottom of the cloud as well, albeit a factor of 20 lower due to extinction by the cloud. We assume that the other background signals are negligible, i.e. the lidar is operating at night and there is no “dark current”.

Multiple scattering was calculated to fourth order using the Eloranta (1998) formulation, assuming a lidar half-angle beam divergence and field-of-view of 0.0258 mrad, which yields a footprint of 20 m at the height of the cloud. Note that this method does not simulate the “bleeding” effect below cloud due to the increased path length of multiply scattered photons. The sensitivity of the retrievals to variations in k with height was examined fully in Blind Test 1, so here k was kept constant with height, although a different value (unknown to the algorithms) was used in each profile.

The final step in generating realistic lidar measurements is to add instrument noise, which we calculate assuming the lidar receiver to be a photon counter. For the resolution considered here (10 km horizontally and 100 m vertically), a single photon detected by the EarthCARE lidar would correspond to a backscatter coefficient of $7 \times 10^{-8} \text{ m}^{-1} \text{ sr}^{-1}$. Fluctuations have been applied accordingly, based on Poisson statistics, such that the reported values of measured attenuated backscatter coefficient are quantized into multiples of $7 \times 10^{-8} \text{ m}^{-1} \text{ sr}^{-1}$. The resulting error is proportional to the square root of the mean, and hence the *relative* error decreases at higher signal levels; this is apparent in Fig. 1.2.

Source of error	Effect				
	α	r_e	IWC	Long-wave	Short-wave
Any error in lidar calibration	no effect	no effect	no effect	no effect	no effect
Radar calibration: reflectivity a factor of 2 too high	no effect	+5 μm	+10%*	< 2 W m^{-2}	+2%*
Any change in absolute value of k	no effect	no effect	no effect	no effect	no effect
k varying by a factor of 2 in a profile	$\pm 25\%^\dagger$	$\pm 2.5 \mu\text{m}^\dagger$	$\pm 25\%^\dagger$	< 2 W m^{-2}	$\pm 5\%*$
Ignoring small crystals in size distribution	no effect	+15%*	+15%*	< 2 W m^{-2}	+3%*
Uncertainties in mass-size relationship	no effect	+30%	+30%	< 2 W m^{-2}	+6%
Non-Rayleigh radar scattering: true $r_e > 100 \mu\text{m}$	no effect	$\simeq 70 \mu\text{m}^\ddagger$	-40%*	< 2 W m^{-2}	+10%*
Neglecting lidar multiple scattering	-60%*	+7 μm^*	+20%*	-60%*	-85%*
Lidar instrument noise spanning a factor of 2	$\pm 35\%^\dagger$	$\pm 3 \mu\text{m}^\dagger$	$\pm 35\%^\dagger$	< 2 W m^{-2}	< 2 W m^{-2}

*Very approximate value.

[†]These errors are fluctuations around the true value, so may largely cancel when integrated quantities are calculated.

[‡]Retrieved effective radius stays constant at around this value.

Table 1.1: Summary of the approximate effect of various factors on the retrieved extinction coefficient (α), effective radius (r_e), ice water content (IWC), long-wave cloud radiative effect and short-wave cloud radiative effect. Note that radiative effects expressed as a percentage indicate the fractional change in the cloudy minus clear-sky fluxes.

Profile	Outgoing long-wave radiation (W m^{-2})	Reflected short-wave radiation (W m^{-2})	Net absorbed radiation (W m^{-2})
Effect of ice	-65.7	+83.9	-18.2
1 Effect of liquid water	-25.2	+108.7	-83.5
Effect of ice and liquid water	-75.8	+139.5	-63.7
Effect of ice	-40.2	+52.5	-12.8
2 Effect of liquid water	-23.5	+111.8	-88.4
Effect of ice and liquid water	-54.0	+127.4	-73.3
Effect of ice	-11.0	+21.0	-10.0
3 Effect of liquid water	-56.1	+190.0	-133.9
Effect of ice and liquid water	-57.3	+194.1	-136.9

Table 1.2: Effects on top-of-atmosphere radiation parameters of ice cloud only, liquid water cloud only, and both ice and liquid water clouds.

1.4 Results

Rather than present all the retrieved parameters for both blind tests and both algorithms, we examine each of the various sources of error in turn and present selected profiles that demonstrate the effect on the retrievals. The findings of this section and the next are summarized in Table 1.1.

1.4.1 Sensitivity to the lidar extinction-to-backscatter ratio

Figure 1.3 shows the true visible extinction coefficient for the profiles of Blind Test 1 and the corresponding values retrieved by the IPSL algorithm. For each of the five profiles there are two retrievals corresponding to the different k profiles used (shown in Fig. 1.1). It can be seen that the retrievals in the

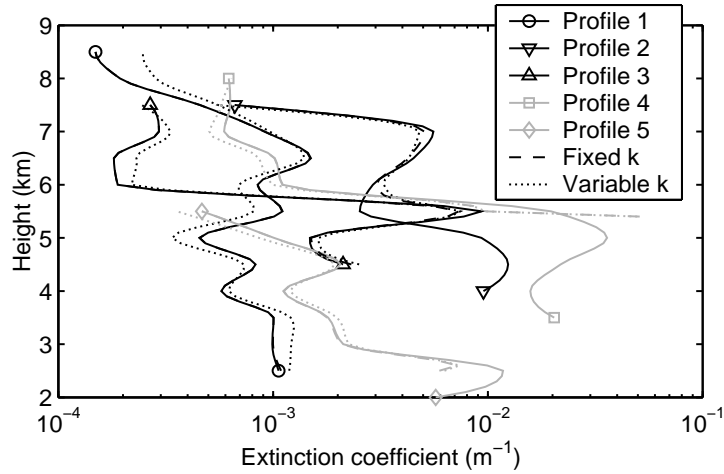


Figure 1.3: Visible extinction coefficient from Blind Test 1: “true” values (solid lines), IPSSL retrieval in the case of constant k with height (dashed lines), and IPSSL retrieval for variable k with height (dotted lines). Note that some of the dashed lines lie directly beneath the solid lines.

case of k constant with height (dashed lines) are remarkably good, in most cases lying directly beneath the “true” curves. For k varying with height (dotted lines), the lidar inversion is still perfectly stable, but it seems that where the local k value is higher than the mean value in the profile by a certain factor then α is underestimated by the same factor (and vice versa).

For both the constant- k and variable- k profiles, the extinction retrievals of the KNMI algorithm (not shown) are almost identical to those of IPSSL. The only difference lies in the lowest few hundred meters of each profile where they begin to diverge and, in the case of constant k with height, diverge from the true extinction as well. The implications of this are examined in the next section.

We next consider the effect of k on the retrievals of ice water content and effective radius. It is clear from (1.1) that any error in the retrieved α will feed through in some way to one or both of these parameters. Figure 1.4 shows a comparison of the true values of IWC and r_e with those derived by the KNMI algorithm, for profiles 1 and 4. Profile 1 shows differences due to non-Rayleigh radar scattering that will be discussed in section 1.4.3, so we consider profile 4, which is representative of the other three profiles of Blind Test 1. The gray dashed and dot-dashed lines show the retrievals in the case of k constant and varying with height respectively (note that in these cases the algorithm has assumed the same mass-size relationship as was used in generating the profiles). It can be seen that between 6 and 7 km, the retrieval with constant k underestimates r_e by around $4 \mu\text{m}$, but the difference between the constant- k and variable- k retrievals is only $1 \mu\text{m}$ (i.e. 2%). Figure 1.3 shows that the corresponding difference in α at this location was 20%. This demonstrates the point made at the start of section 1.2 that retrieved particle size should be very insensitive to errors in either Z or α . In Fig. 1.4 it can be seen that this 20% underestimate in α corresponds to an underestimate in IWC by about the same amount.

1.4.2 Sensitivity to lidar extinction correction technique

Blind Test 1 should be regarded as a very stringent test of the algorithms; by providing them with attenuated lidar backscatter values down to $10^{-10} \text{ m}^{-1} \text{ sr}^{-1}$, their potential ability to correct for one-way optical depths of up to 7 (i.e. to recover signals depleted by a factor of 10^6) has been evaluated. The results reported in the last section are very encouraging, with both algorithms able to recover extinction accurately through most of the profile (if k varies within a profile and no other a priori information is

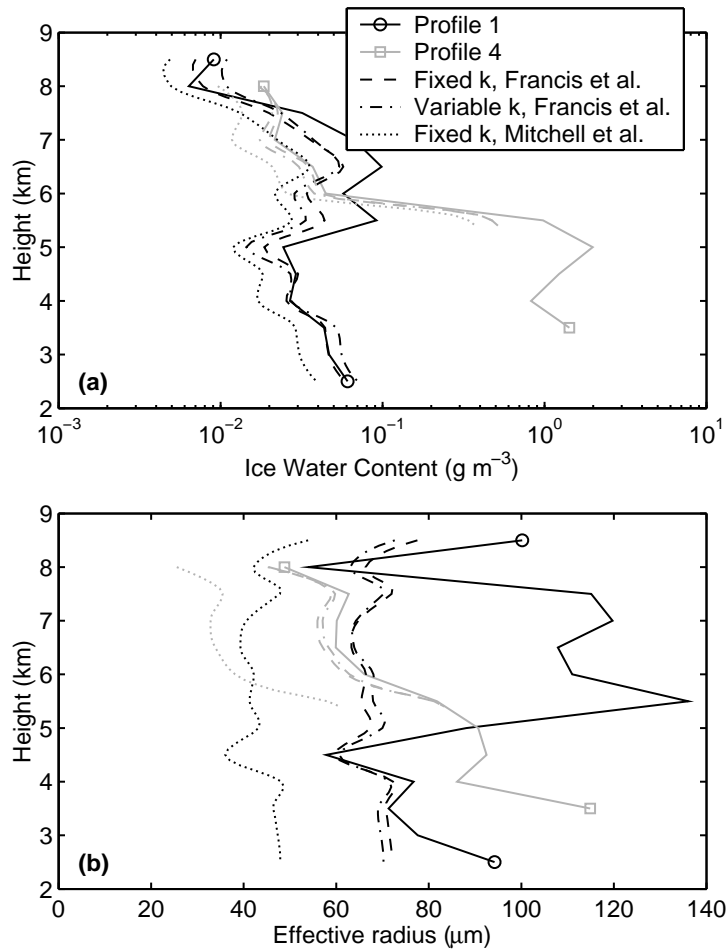


Figure 1.4: Ice water content and effective radius from profiles 1 and 4 of Blind Test 1: “true” values (solid lines), KNMI retrieval assuming the same Francis et al. (1998) mass-size relationship that was used in generating the profiles (dashed lines), and KNMI retrieval assuming the different Mitchell et al. (1996b) mass-size relationship (dotted lines).

available on the nature of the cloud then the biases evident in Fig. 1.3 are probably unavoidable). The difference in algorithm behaviour shown in Table 1.3 are due to whether r'_e or N_0^* is assumed to be constant in the region where the lidar loses signal.

Table 1.3 shows the true optical depth of each of the profiles and the associated errors in the retrieved values in the case of k constant with height. Of course, where the lidar loses signal in the middle of the cloud it is impossible to estimate the full optical depth, so columns 4 and 5 show the errors in the estimate of optical depth down to the depth of the lowest measurable lidar return. Considering Blind Test 1, the mean absolute error is 0.93 (14%) for the KNMI algorithm and 0.56 (9%) for the IPSL algorithm, seemingly higher than the errors indicated by the dashed lines in Fig. 1.3. However, most of this error occurs in the lowest 400 m of the cloud (or the last 400 m that the lidar has a signal), where the assumption of r'_e or N_0^* constant has most effect on the retrieval. The last two columns of Table 1.3 show that, when the lowest 400 m of the profile is excluded from the calculation of optical depth, the error is much less (around 0.2, or 5%) in Blind Test 1. The KNMI errors in Blind Test 2 are around twice as large, possibly due to difficulties with the boundary assumptions when multiple scattering degrades the lidar signal. The large IPSL errors in Blind Test 2 are due to uncorrected multiple scattering, discussed

Profile	Full optical depth	Optical depth to lidar penetration			Opt. depth to lidar penetration –400 m		
		True	KNMI error	IPSL error	True	KNMI error	IPSL error
1	4.739	4.739	+0.120	+0.002	4.326	+0.041	–0.006
2	21.670	7.157	–0.057	+0.216	6.092	–0.342	–0.331
3	5.002	5.002	–0.888	–0.392	4.300	–0.588	–0.434
4	52.908	8.331	–2.885	+1.205	2.060	–0.012	–0.013
5	11.830	7.231	–0.706	–1.009	3.992	–0.040	–0.042
<i>Mean absolute error (profiles 1–5):</i>			0.93 (14%)	0.56 (9%)		0.20 (5%)	0.17 (4%)
6	13.858	3.640	+1.437	–3.061	2.881	+0.039	–2.330
7	22.267	3.525	+0.803	–2.477	2.693	+0.230	–1.697
8	1.421	1.421	+0.209	–0.924	1.407	+0.195	–0.938
9	8.016	4.031	+0.471	–3.185	2.679	+0.067	–1.849
10	5.724	5.688	–2.166	–5.011	4.226	–0.891	–3.589
<i>Mean absolute error (profiles 6–10):</i>			1.02 (28%)	2.93 (80%)		0.28 (10%)	2.08 (75%)

Table 1.3: True and retrieved optical depths for Blind Test 1 (profiles 1–5) and Blind Test 2 (profiles 5–6), for constant k with height. The optical depths of the full profile are shown in column 2, but note that only in profiles 1, 3 and 8 did the lidar detect the full extent of the cloud. Column 3 shows the optical depth from cloud top down to the depth of lidar penetration, and columns 4 and 5 show the associated errors in the KNMI and IPSL retrievals. As most of the retrieval error occurs in the lowest 400 m, column 6 shows the optical depth down to 400 m above the lidar penetration depth, with the errors in the retrievals down to this depth in columns 7 and 8. Note that the large errors in the IPSL retrievals in profiles 6–10 are due to its neglect of multiple scattering in Blind Test 2 (see section 1.4.5).

in section 1.4.5. In section 1.5 the sensitivity of the radiative fluxes to these various errors is evaluated.

These differences in optical depth suggest that refinements could be made to the extinction-correction procedure. The lower mean error in the IPSL retrievals in Blind Test 1 suggests that it may be more realistic to consider N_0^* constant at the far end of the cloud than r_e' , although it should be stressed that the aircraft data used here do not represent true vertical profiles so the behaviour of r_e' and N_0^* at cloud base is not necessarily realistic. One approach would be to use a cost function that penalizes gradients in both N_0^* and r_e' . The retrieved extinction of profile 4 in Fig. 1.3 exhibits a sharp overestimate in the lowest few hundred metres of the cloud, suggesting that penalizing sharp gradients in extinction would also be worthwhile. Either more aircraft data or actual ground-based radar-lidar retrievals would have to be studied to determine the best form of such a cost function.

1.4.3 Sensitivity to non-Rayleigh radar scattering

The retrieval of particle size is possible because Z is a much higher moment of the size distribution than α . However, at high radar frequencies such as 94 GHz, a problem occurs when large particles are present as they no longer scatter according to the Rayleigh approximation (i.e. $\gamma < 1$ in Eq. 1.3). While this can be taken into account to some degree by the retrieval algorithms, it was shown by Hogan et al. (2003) that for an effective radius greater than around 90 μm and assuming the Francis et al. (1998) mass-area relationship, the non-Rayleigh scattering effectively renders Z a *lower* moment of the distribution than α and all further capability to infer particle size is lost.

The problem is demonstrated in Fig. 1.4. While profile 4 shows excellent agreement between “truth” (solid line) and retrieval (dashed line), in both IWC and r_e , the retrieval in profile 1 predicts r_e values of around 70 μm when the true values are closer to 140 μm . Since the α profile is still retrieved very accurately, it is clear from (1.1) that IWC must also be underestimated by around a factor of 2, and

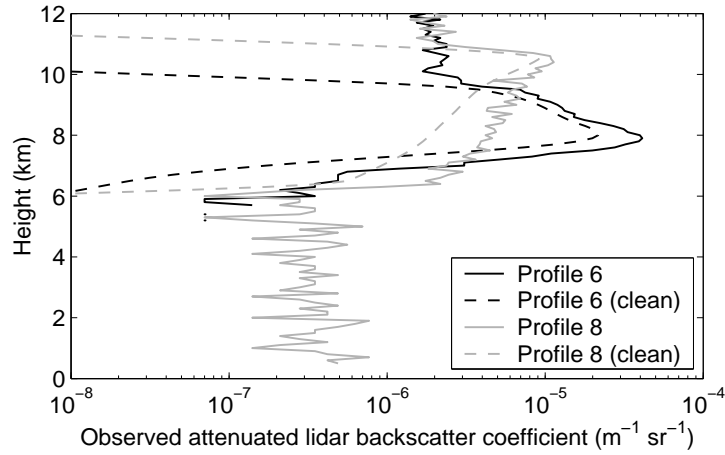


Figure 1.5: Observed attenuated backscatter coefficient from profiles 6 and 8 of Blind Test 2 (solid lines) together with the “clean” profiles that would have been observed in the absence of multiple scattering, molecular scattering and instrument noise (dashed lines).

this is indeed what is found. This problem seems unavoidable at 94 GHz, and while a solution from the ground is to use a lower frequency, such as 35 GHz, requirements on sensitivity, beamwidth and power consumption mean that this solution is unlikely to be considered from space.

1.4.4 Sensitivity to the mass-size relationship

The mass-size relationship of Francis et al. (1998) was used to generate all the profiles in Blind Test 1 and (coincidentally) was also used in the IPSL retrievals. The KNMI algorithm was run twice for each profile, once assuming the Francis et al. relationship and once assuming the “planar polycrystal” relationship of Mitchell et al. (1996b), thereby enabling the effect of changes in mass-size relationship to be tested.

The first thing to note is that the retrieval of extinction coefficient is essentially independent of assumptions on the size distribution or the mass-size relationship. As discussed in section 1.2.3, both algorithms retrieve extinction simply by minimizing the variation with height of the ratio of some power of Z to some power of α , and the near identical results from the two algorithms indicates that the actual powers used are not particularly important for most of the depth of the cloud.

The dotted lines in Fig. 1.4 demonstrate the effect of assuming a different mass-size relationship in the retrieval to that of the “real” cloud. In this case both IWC and r_e are underestimated by 30%. It should be noted that other radar-based retrieval algorithms are also sensitive to this uncertainty. The significance of errors in IWC and r_e of this magnitude for radiative fluxes is explored in section 1.5.2.

1.4.5 Sensitivity to lidar multiple scattering

The effect of multiple scattering, molecular scattering and instrument noise on the direct lidar measurements is demonstrated in Fig. 1.5, which shows two of the profiles from Blind Test 2 together with the profiles that would have been observed in the absence of these effects (i.e. using the Blind Test 1 method). The effect of multiple scattering is clearly apparent as an enhancement of the observed backscatter that increases with range as the lidar beam penetrates further down into the cloud, reaching in excess of a factor of 5 at the location of the lowest lidar echo.

Figure 1.6 shows the true extinction profiles for these two cases, together with the retrievals by the

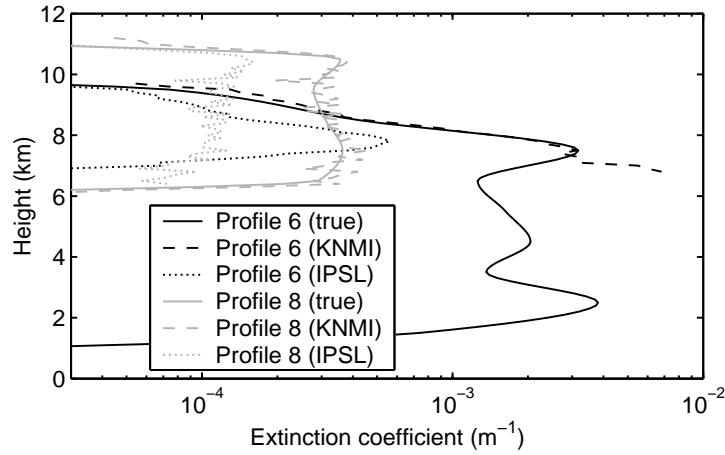


Figure 1.6: Visible extinction coefficient for profiles 6 and 8 of Blind Test 2: “true” values (solid lines), KNMI retrievals accounting for the effect of multiple scattering (dashed lines) and IPSL retrievals neglecting the effect of multiple scattering (dotted lines).

two algorithms. The KNMI algorithm performs very well, demonstrating that it is possible to account for the strong effect of multiple scattering. It should be noted that the test is somewhat unrealistic as the Eloranta (1998) multiple-scattering approximation was used in both the simulation and the retrieval. A more stringent test would be to use a Monte Carlo calculation in the simulation of the lidar observations. In this way the increased path length of the multiply scattered photons would exhibit itself as a “bleeding” effect in range at the far end of the cloud, which is not represented in the Eloranta formulation. This phenomenon was particularly noticeable behind liquid clouds observed during the Lidar In-space Technology Experiment, LITE (Winker et al. 1996). It should be noted that this effect tends to be much less significant in ice clouds, and the large 300-m footprint of LITE will have exacerbated the problem compared to 20–35 m footprint proposed for EarthCARE.

The effect of neglecting multiple scattering in the retrieval is shown by the IPSL profiles in Fig. 1.6, which underestimate extinction by a factor of 2.5 at cloud top, increasing to a factor of 4 at cloud base. In Table 1.3 it can be seen that the underestimate in total cloud optical depth is around 80%. It might seem counter-intuitive that when the observed backscatter is higher than in the case of no multiple scattering, the algorithm produces an extinction that is too low. The crucial point here is that it is the gradient in β' that is used by the algorithm, not the absolute value itself. Figure 1.5 shows that multiple scattering has the effect of making the backscatter decrease less rapidly with range, which the retrieval algorithm interprets as being due to weaker extinction of the beam by the cloud. This underestimate of extinction constitutes the largest error in Table 1.1, highlighting that it is essential for multiple scattering to be accounted for in any algorithm. Work is currently underway to incorporate a multiple scattering correction into the IPSL algorithm.

1.4.6 Sensitivity to instrument noise and molecular scattering

The lidar instrument noise evident in Fig. 1.6 appears as fluctuations in the retrieved extinction in Fig. 1.6, but crucially does not seem to have affected the stability of the inversion. The corresponding effective radius profiles are shown in Fig. 1.7. The systematic differences are discussed in the next section, but here the important thing to note is the much lower fluctuation of retrieved r_e than α . This is due to the insensitivity of retrieved size to errors in α discussed earlier. Therefore, by (1.1), fluctuations tend to be

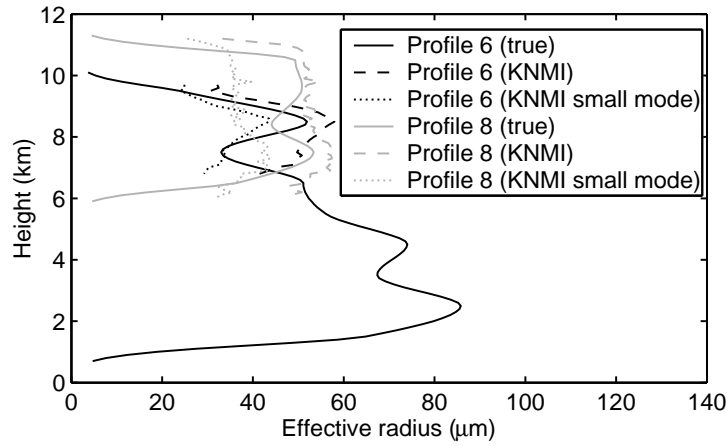


Figure 1.7: Effective radius for profiles 6 and 8 of Blind Test 2: “true” values (solid lines), standard KNMI retrieval (dashed lines), and KNMI retrieval assuming the presence of a small crystal mode in the size distribution (dotted lines).

present in IWC of a similar magnitude to those in α .

Instrument noise also effectively sets a limit on the sensitivity of the lidar, and thus to the depth into the cloud that the algorithm can be applied. It should be noted that the fluctuations simulated are specific to a photon counter. As is evident in Fig. 1.2, the radar instrument noise is negligible compared to the lidar noise, and therefore its specific effect cannot be detected in the retrievals. Molecular scattering does not seem to have had any detectable effect on the retrievals, and with the radar available, distinguishing cloud from purely molecular scattering regions will usually be straightforward.

1.4.7 Sensitivity to the shape of the size distribution

As with the mass-size relationship, the shape of the size distribution has no effect on the retrieval of extinction so we concentrate on IWC and r_e . Profile 4 in Fig. 1.4 seems to indicate that in the absence of other sources of error (such as variable k or a different mass-size relationship being used in the simulation and the retrieval), IWC and r_e can be retrieved to within 5%; similar accuracies were seen for profiles 2–5 of Blind Test 1 (profile 1 being adversely affected by non-Rayleigh radar scattering). This can be regarded as the “residual” error due to uncertainties in the size distribution. It is surprisingly low given that the spectra used in Blind Test 1 are known to be distinctly bimodal. However, it was only in Blind Test 2 that a correction was made to counter the problem of undercounting of small crystals by the 2D cloud probe.

Figure 1.7 shows effective radius from profiles 6 and 8 of Blind Test 2. Two KNMI retrievals are shown for each case, one using assuming that the size distribution may be represented by a gamma distribution, and the other assuming the presence of an additional small ice crystal mode in the distribution following the work of Mitchell et al. (1996a). Without the small crystal mode, the retrieval overestimates r_e by on average 15%, and with the correction it tends to be underestimated by the same amount. We can surmise that the small mode added in the KNMI algorithm is twice as strong as the gamma distribution fitted to the EUCREX size spectra to generate the profiles of Blind Test 2 (see section 1.3.2). The variability in the small mode in the size spectra of ice clouds is an area of active research, but it would seem from this study that there is an error of at least 15% in both retrieved r_e and IWC, due to uncertainties in the nature of the size distribution.

1.4.8 Sensitivity to instrument calibration

While errors in instrument calibration were not simulated in the Blind Tests, from the equations involved and what has been learned so far, it is possible to determine the effect they would have on the retrievals. In the case of the radar, a calibration offset would not affect the extinction correction described in sections 1.2.2 and 1.2.3, because only the fractional variation of Z with range is considered. The retrieval of IWC and r_e would be affected, however. If the Francis et al. (1998) mass-area relationship is assumed then Fig. 12 of Hogan et al. (2003) shows that for r_e between $20\ \mu\text{m}$ and $80\ \mu\text{m}$, a factor of 10 increase in the ratio Z/α corresponds to an increase in r_e of $17\ \mu\text{m}$. Therefore a factor-of-2 overestimate of Z would result in a $5\ \mu\text{m}$ overestimate of r_e .

By contrast, lidar calibration has no effect on any of the retrieved parameters. This is because it is only relative changes in β' that are used in the retrieval, the absolute value is not important. This fact is illustrated by noting that changing the lidar calibration would have the same effect as multiplying k by a constant factor through the whole profile, and it has already been shown that the retrieval of extinction is complete insensitive to the absolute value of k .

1.5 Radiation calculations

1.5.1 Introduction

We have shown that, provided multiple scattering can be accounted for, the combination of radar and lidar has the capability to retrieve extinction coefficient very accurately, but with errors in the furthest few hundred metres resulting in total cloud optical depth sometimes being wrong by more than 1. Effective radius and ice water content, show sensitivity to several factors, namely (in order of importance) non-Rayleigh scattering for $r_e > 90\ \mu\text{m}$, the mass-size relationship, the shape of the size distribution and radar calibration. While IWC tends to be cited as the ice-cloud parameter in models that is in most need of evaluation (e.g. Stephens et al. 2002), it is principally for their radiative effects that clouds are important and it is not immediately obvious how errors in these three parameters feed through to uncertainties in radiative fluxes.

This section describes the results of radiative flux calculations performed on the “true” and retrieved profiles, which we use to assess the radiative implications of the various sensitivities found in section 1.4. For brevity, only one representative profile is shown from each of the Blind Tests, but this is sufficient to illustrate the effect of all the various factors.

The Edwards and Slingo (1996) radiation code is used, assuming a solar zenith angle of 60° , a surface albedo of 0.2 and no low cloud present. Thus the top-of-atmosphere downwelling solar flux is $685\ \text{W m}^{-2}$ in each profile. The clouds are assumed to be horizontally homogeneous and are embedded in the McClatchey et al. (1972) standard mid-latitude summer atmosphere, using the aircraft-observed temperatures in the cloud and the values from the standard atmosphere above and below. Relative humidity was set to 100% with respect to ice within the cloud. The long-wave calculations employed 9 spectral bands and used the Slingo and Schrecker (1982) parameterization for the ice particle properties, while the short-wave used 24 bands together with the Kristjánsson et al. (2000) scheme.

1.5.2 Example from Blind Test 1: profile 3

The first case considered is the KNMI retrieval of profile 3 of Blind Test 1, in which the full extent of the cloud was detected by the lidar. We first consider the “best case”, i.e. constant k and the same Francis et al. (1998) mass-size relationship being used in the simulation and the retrieval. This is shown by the

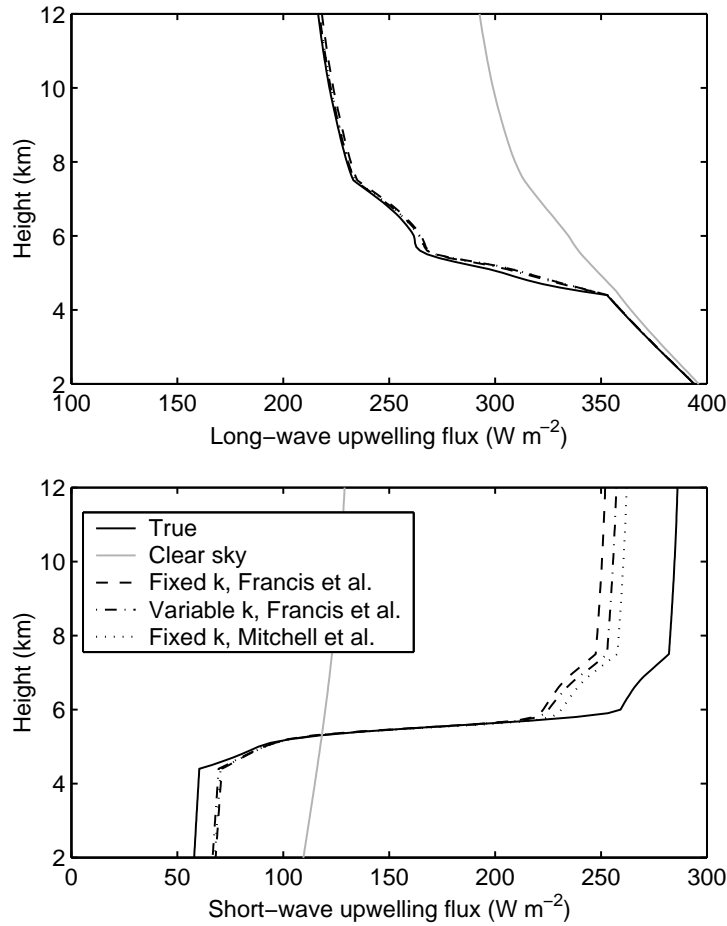


Figure 1.8: Upwelling fluxes from profile 3 of Blind Test 1, calculated both from the “true” profile and three different KNMI retrievals.

dashed lines in Fig. 1.8. In the long-wave the agreement is striking, with a difference of only around 2 W m^{-2} in outgoing long-wave radiation (OLR), and little more at any point in the profile. In the short-wave, however, the upwelling top-of-atmosphere (TOA) flux is underestimated by 35 W m^{-2} (or 20% when expressed as a fraction of the cloudy minus clear-sky upwelling fluxes), with the difference apparently originating at a height of between 5 and 6 km. The problem can be identified in Table 1.3, which shows that the KNMI algorithm underestimated optical depth by 0.9 (20%), and likewise in Fig. 1.3 we see that the magnitude of the strong spike in α at 5.5 km is underestimated by around 20%. As this is the most optically thick part of the cloud, it is the region most sensitive to errors. This initial test has clearly demonstrated the large difference between the behaviour of the short-wave and long-wave fluxes: in the short-wave the reflected flux is sensitive to the total optical depth of the cloud, while in the longwave the dependence quickly “saturates”, and the cloud behaves as a black body. Note that errors in downwelling surface short-wave radiation are typically of the same magnitude as the errors in upwelling TOA short-wave. Additionally, since the relationship between optical depth and short-wave cloud albedo has not saturated for the modest optical depths considered here, we may easily estimate the errors in short-wave fluxes for the other profiles from the errors in optical depth listed in Table 1.3.

We next consider the effect of a variable k profile. In Fig. 1.3 it can be seen that in this particular case, variable k led to an overestimate of α by around 25% in the top-most 1.5 km of the cloud, although the total optical depth was still underestimated by 0.620 (as opposed to 0.888 for the constant k profile).

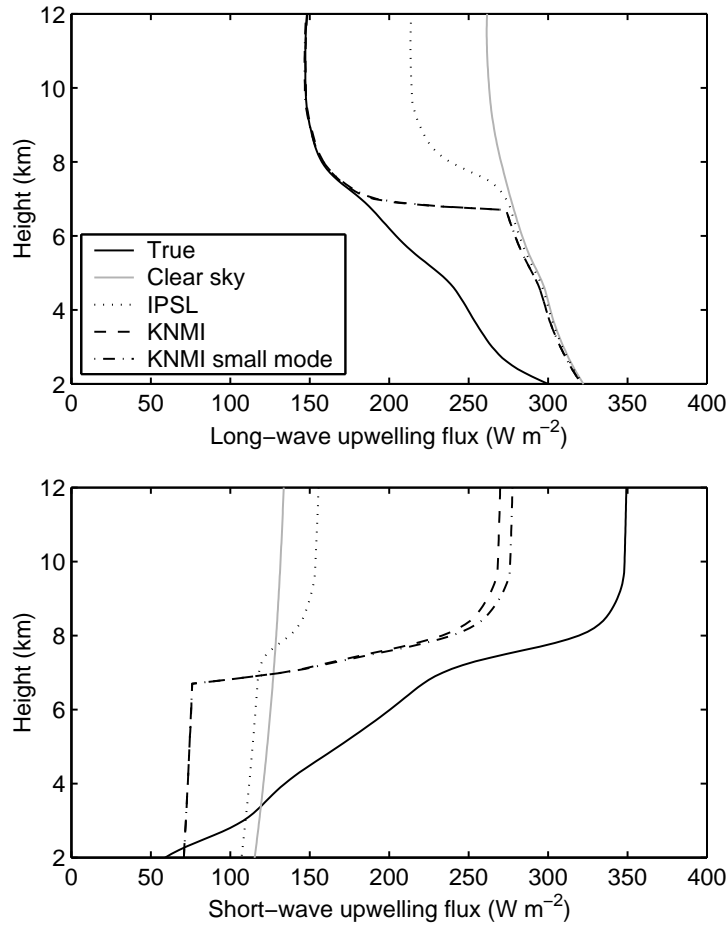


Figure 1.9: Upwelling fluxes from profile 6 of Blind Test 2.

The effect on the radiation is consequently quite small, a decrease of 1 W m^{-2} in the long-wave and an increase of 6 W m^{-2} in the short-wave. If we express these changes relative to the clear-sky upwelling flux, the values become 2% and 5%. In the long-wave the cloud is still acting very much as a black body, while in the short-wave the total optical depth is important, with the vertical location of the most optically thick parts of the cloud being virtually irrelevant.

Figure 1.8 also shows the fluxes corresponding to the Mitchell et al. (1996b) polycrystal assumption being used in the KNMI algorithm. As in all the profiles of Blind Test 1, this assumption results in a 30% reduction in the retrievals of both r_e and IWC, although of course α is unaffected. However, it is interesting that it appears to have only a 5% effect in the short-wave and a negligible effect in the long-wave. This highlights the critical point that extinction coefficient is much the most important parameter in determining the radiative fluxes in both the long-wave and short-wave. Effective radius (and from Eq. 1.1, IWC) determines the single-scatter albedo and asymmetry factor of the particles, but this plays a much less significant role. We may regard it as fortunate, therefore, that the extinction profile is what is retrieved with most accuracy by combined radar and lidar.

1.5.3 Example from Blind Test 2: profile 6

Figure 1.9 depicts the upwelling fluxes calculated for profile 6 of Blind Test 2. The full extent of this particular profile was not detected by the lidar so no retrieval was possible in the lowest part of the

cloud, but nonetheless this case illustrates several important points. Firstly it can be seen that the OLR predicted by the KNMI algorithm is accurate to better than 1 W m^{-2} despite only the top 1 km or so being retrieved. This highlights again the fact that OLR is only really sensitive to extinction coefficient near the top of the cloud, and certainly the depth of penetration of a lidar with realistic sensitivity is more than adequate to characterize enough of the cloud. By contrast, the short-wave upwelling TOA flux is underpredicted by 80 W m^{-2} , since in the short-wave the full optical depth is important.

The impact of neglecting multiple scattering is clearly exposed in the comparison of the KNMI and IPSL retrievals. The long-wave effect of the cloud retrieved by the IPSL algorithm is less than half that of the cloud retrieved by the KNMI algorithm, and the difference in the short-wave is even more stark. This is to be expected given the underestimate of extinction shown in Fig. 1.6.

Next the effect of assumed size distribution is examined. In Fig. 1.7 it can be seen that the inclusion of a “small mode” in the KNMI algorithm results in a 30% reduction in predicted r_e (and IWC). In Fig. 1.9b it can be seen that this results in only a 7% increase in the effect of the cloud in the short-wave close to the 5% found for the same change in r_e in section 1.5.2. So for this configuration of the radiation code we can say that for a fixed extinction profile, the fractional change in the effect of a retrieved cloud on the shortwave fluxes would be around 20% of any fractional change in r_e . By contrast, for the modest optical depths considered here there is an approximately linear relationship between short-wave cloud albedo and optical depth for constant r_e .

In profile 6 of Fig. 1.6 it can be seen that just before the lidar loses signal at around 7 km, the KNMI retrieval produces an erroneous “spike” in extinction, up to 5 times greater than the true value. Admittedly the error bar that would be reported by the algorithm for these last few points would be high, but it is worthwhile commenting on the effect on the radiation field. In Fig. 1.9 both the long-wave and short-wave fluxes show a very sharp gradient at 7 km, which when the downwelling fluxes are also considered corresponds to a heating rate of 60 K d^{-1} . This is an unrealistically high value for ice clouds and highlights the need for algorithms to ensure stability at all locations. One solution (also discussed in section 1.4.2) would be to add a term to the cost function used in section 1.2.2 to penalize sharp changes in α as well as in r'_e or N_0^* .

1.6 Conclusions

In this chapter the ability of spaceborne radar and lidar synergy to retrieve the important microphysical parameters of ice clouds has been independently tested, with specific examination of the sensitivities to numerous different sources of error, summarized in Table 1.1. The main strength of the technique is the accuracy of the retrieved extinction profile and its insensitivity to assumptions on the nature of the size distribution, the habit of the particles or errors in instrument calibration. Long-wave fluxes calculated from the derived profiles are found to be remarkably accurate, with errors of the order of 2 W m^{-2} . Further work is nonetheless required to refine the extinction retrieval in the lowest 400 m before the lidar loses signal, in order that the accuracy of inferred optical depth (and consequently the short-wave fluxes) is improved. It should be noted that lidar detection of the air molecules can also be used to infer the extinction profile accurately, either using the molecular return at the far side of the cloud (Klett 1985) or throughout the cloud with a high spectral resolution lidar (ESA 2001). However, these techniques are limited to much less optically thick clouds than the radar-lidar algorithm.

Clearly the fact that the radar-lidar algorithm is only applicable where the lidar has a detectable cloud signal (i.e. in the top 3–5 optical depths of the cloud), and the consequent errors in predicted short-wave fluxes, means that it will be necessary to fall back on a radar-only retrieval of cloud properties in

the lower part of many of the thicker ice clouds. Further work is required to find the optimum way to “blend” the two types of retrieval.

Retrievals of ice water content and effective radius are sensitive to the assumed ice particle mass-size relationship, and to a lesser extent to the presence of small ice crystals, although these factors play a much less significant role in determining the radiative fluxes than extinction. It should be pointed out that these problems are common to all radar algorithms (e.g. Matrosov et al. 2002, Hogan et al. 2000), but without the accurate retrieval of extinction available from the inclusion of lidar information, the inferred radiative fluxes would be expected to be much less accurate.

We have demonstrated that it is essential for the effects of lidar multiple scattering to be corrected for as part of the retrieval; for the EarthCARE configuration the neglect of this effect results in optical depth being underestimated by around 80%. Further tests using full Monte Carlo calculations would need to be performed to ensure that the use of the simpler Eloranta (1998) formulation is adequate to use in the retrieval algorithm.

Two additional effects have not been considered in this chapter yet are important if the technique is to be implemented successfully from space. Firstly, the radar and lidar should be well aligned in order that they are sampling the same region of cloud. In the case of EarthCARE this is not an issue as both instruments are mounted on the same platform, but for CloudSat and Calipso, the orientation of the two satellites will have to be monitored and adjusted very carefully. Illingworth et al. (2000) estimated that in a typical mid-latitude cirrus cloud for 10-km along track integration, a lateral instrument separation of 2 km would lead to retrieval errors of the order of 25%, rising to a factor of two for a separation of 10 km.

The second issue is that of specular reflection from horizontally aligned plate crystals, which can occur when ice clouds are observed by lidar within 1° of zenith or nadir (Thomas et al. 1990). This has the effect of increasing the apparent lidar backscatter but with no associated increase in extinction, i.e. a dramatic reduction in k . If these crystals were distributed evenly in the vertical then it would be of no concern, as in section 1.4.1 the insensitivity of the results to the absolute value of k was demonstrated. However, specular reflection occurs preferentially in layers where plate crystals predominate, such as between -9°C and -23°C , with the result that variations in k in a single profile would span a considerably wider range than those in Fig. 1.1c, and the resulting biases in retrieved extinction would be more severe. It would therefore be very advantageous for the lidar to point a few degrees from nadir to eliminate this effect completely.

To conclude, the concept of using “blind tests” based around aircraft-simulated profiles has been a very successful one, and would be well suited to testing other retrieval algorithms, including combinations of active and passive sensors.

References

- Ansmann, A., U. Wandinger, M. Riebesell, C. Weitkamp and W. Michaelis, 1992: Independent measurement of extinction and backscatter profiles in cirrus clouds by using a combined Raman elastic-backscatter lidar. *Appl. Optics*, **33**, 7113–7131.
- Brown, P. R. A., and P. N. Francis, 1995: Improved measurements of the ice water content in cirrus using a total-water probe. *J. Atmos. Oceanic Technol.*, **12**, 410–414.
- Brown, P. R. A., A. J. Illingworth, A. J. Heymsfield, G. M. McFarquhar, K. A. Browning and M. Gosset, 1995: The role of spaceborne millimeter-wave radar in the global monitoring of ice-cloud. *J. Appl. Meteorol.*, **34**, 2346–2366.
- Donovan, D. P., and A. C. A. P. van Lammeren, 2001: Cloud effective particle size and water content profile retrievals using combined lidar and radar observations - 1. Theory and examples. *J. Geophys. Res.*, **106**, 27 425–27 448.
- Edwards, J. M., and A. Slingo, 1996: Studies with a flexible new radiation code - 1. Choosing a configuration for a large scale model. *Quart. J. Roy. Meteorol. Soc.*, **122**, 689–719.

- Eloranta, E. W., 1998: A practical model for the calculation of multiply scattered lidar returns. *Appl. Optics*, **37**, 2464–2472.
- European Space Agency (ESA), 2001: *EarthCARE - Earth Clouds, Aerosols and Radiation Explorer*. ESA SP-1257 (1)—The five candidate Earth Explorer Core Missions, ESA/ESTEC, Noordwijk, The Netherlands.
- Field, P. R., 2000: Bimodal ice spectra in frontal clouds. *Quart. J. Roy. Meteorol. Soc.*, **126**, 379–392.
- Foot, J. S., 1988: Some observations of the optical properties of clouds - 2. Cirrus. *Quart. J. Roy. Meteorol. Soc.*, **114**, 145–164.
- Francis, P. N., P. Hignett and A. Macke, 1998: The retrieval of cirrus cloud properties from aircraft multi-spectral reflectance measurements during EUCREX'93. *Quart. J. Roy. Meteorol. Soc.*, **124**, 1273–1291.
- Heymsfield, A. J., and D. G. Baumgardner, 1985: Summary of workshop on processing 2-D probe data. *Bull. Am. Meteorol. Soc.*, **66**, 437–440.
- Hogan, R. J., and A. J. Illingworth, 1999: The potential of spaceborne dual-wavelength radar to make global measurements of cirrus clouds. *J. Atmos. Oceanic Technol.*, **16**, 518–531.
- Hogan, R. J., and A. J. Illingworth, 2003: Parameterizing ice cloud inhomogeneity and the overlap of inhomogeneities using cloud radar data. *J. Atmos. Sci.*, **60**, 756–767.
- Hogan, R. J., A. J. Illingworth and H. Sauvageot, 2000: Measuring crystal size in cirrus using 35- and 94-GHz radars. *J. Atmos. Oceanic Technol.*, **17**, 27–37.
- Hogan, R. J., P. N. Francis, H. Flentje, A. J. Illingworth, M. Quante and J. Pelon, 2003: Characteristics of mixed-phase clouds - 1. Lidar, radar and aircraft observations from CLARE'98. *Quart. J. Roy. Meteorol. Soc.*, **129**, 2089–2116.
- Illingworth, A. J., and T. M. Blackman, 2002: The need to represent raindrop size spectra as normalized gamma distributions for the interpretation of polarization radar observations. *J. Appl. Meteorol.*, **41**, 287–297.
- Illingworth, A. J., R. J. Hogan, A. C. A. P. van Lammeren, D. P. Donovan, F. H. Berger, T. Halecker, C.-L. Liu, A. Feijt and H. I. Bloemink, 2000: *Quantification of the synergy aspects of the Earth Radiation Mission*. Final report, ESTEC Contract 13167/98/NL/GD.
- Intrieri, J. M., G. L. Stephens, W. L. Eberhart and T. Uttal, 1993: A method for determining cirrus cloud particle sizes using lidar and radar backscatter techniques. *J. Appl. Meteorol.*, **32**, 1074–1082.
- Klett, J. D., 1985: Lidar inversion with variable backscatter/extinction ratios. *Appl. Optics*, **24**, 1638–1643.
- Kristjánsson, J. E., J. M. Edwards and D. L. Mitchell, 2000: Impact of a new scheme for optical properties of ice crystals on climates of two GCMs. *J. Geophys. Res.*, **105**, 10 063–10 079.
- Liou, K.-N., 1986: Influence of cirrus clouds on weather and climate processes: A global perspective. *Monthly Weather Rev.*, **114**, 1167–1199.
- Liu, C.-L. and A. J. Illingworth, 2000: Towards more accurate retrievals of ice water content from radar measurement of clouds. *J. Appl. Meteorol.*, **39**, 1130–1146.
- Mace, G. G., K. Sassen, S. Kinne and T. P. Ackerman, 1999: An examination of cirrus cloud characteristics using data from millimeter wave radar and lidar: The 24 April SUCCESS case study. *Geophys. Res. Lett.*, **25**, 1133–1136.
- Matrosov, S. Y., A. V. Korolev and A. J. Heymsfield, 2002: Profiling cloud ice mass and particle characteristic size from Doppler radar measurements. *J. Atmos. Oceanic Technol.*, **19**, 1003–1018.
- McClatchey, R. A., R. W. Fenn, J. E. A. Selby, F. E. Volz and J. S. Garing, 1972: Optical properties of the atmosphere (3rd. ed.), Air Force Cambridge Research Laboratories, Rep. No. AFCRL72-0497, L. G. Hanscom Field.
- McFarquhar, G. M., and A. J. Heymsfield, 1997: Parameterization of tropical cirrus ice crystal size distributions and implications for radiative transfer: Results from CEPEX. *J. Atmos. Sci.*, **54**, 2187–2200.
- Mitchell, D. L., S. K. Chai, Y. Liu, A. J. Heymsfield and Y. Dong, 1996a: Modeling cirrus clouds - 1. Treatment of bimodal size spectra and case study analysis. *J. Atmos. Sci.*, **53**, 2952–2966.
- Mitchell, D. L., A. Macke and Y. Liu, 1996b: Modeling cirrus clouds - 2. Treatment of radiative properties. *J. Atmos. Sci.*, **53**, 2967–2988.
- O'Connor, E. J., R. J. Hogan and A. J. Illingworth, 2003: Retrieving stratocumulus drizzle parameters using Doppler radar and lidar. *Submitted to J. Appl. Meteorol.*
- Slingo, A., and H. M. Schrecker, 1982: On the shortwave radiative properties of stratiform water clouds. *Quart. J. Roy. Meteorol. Soc.*, **108**, 407–426.
- Stephens, G. L., S. C. Tsay, P. W. Stackhouse Jr. and P. J. Flatau, 1990: The relevance of the microphysical and radiative properties of cirrus clouds to climate and climatic feedback. *J. Atmos. Sci.*, **47**, 1742–1752.

- Stephens, G. L., D. G. Vane, R. J. Boain, G. G. Macs, K. Sassen, Z. Wang, A. J. Illingworth, E. J. O'Connor, W. B. Rossow, S. L. Durden, S. D. Miller, R. T. Austin, A. Benedetti, C. Mitrescu and the CloudSat Science Team, 2002: The CloudSat Mission and the A-Train. *Bull. Am. Meteorol. Soc.*, **83**, 1771–1790.
- Testud, J., S. Oury, X. Dou, P. Ameyenc and R. Black, 2001: The concept of normalized distribution to describe raindrop spectra: a tool for cloud physics and cloud remote sensing. *J. Appl. Meteorol.*, **40**, 1118–1140.
- Thomas, L., J. C. Cartwright and D. P. Wareing, 1990: Lidar observations of the horizontal orientation of ice crystals in cirrus clouds. *Tellus*, **42B**, 211–216.
- Tinel, C., 2002: *Restitution des propriétés microphysiques et radiatives des nuages froids et mixtes à partir des données du système RALI (radar/lidar)*. PhD Thesis, Université Paris 7.
- Tinel, C., J. Testud, A. Guyot and K. Caillault, 2000: Cloud parameter retrieval for combined remote sensing observations. *Phys. Chem. Earth*, **25**, 1063-1067.
- Wang, Z., and K. Sassen, 2002: Cirrus cloud microphysical property retrieval using lidar and radar measurements - 1. Algorithm description and comparison with in situ data. *J. Appl. Meteorol.*, **41**, 218–229.
- Winker, D. M., R. H. Couch and M. P. McCormick, 1996: An overview of LITE—NASA Lidar In-space Technology Experiment. *Proc. IEEE*, **84**, 164–180.